MNRAS **000**, 1–15 (2015) Preprint 21 May 2023 Compiled using MNRAS LATEX style file v3.0

Population statistics of intermediate-mass black holes in dwarf galaxies using the NewHorizon simulation

Beckmann, R.S.[1]★, Dubois, Y.[2], Volonteri, M.[2], Dong-Páez, C. A.[2], Trebitsch, M.[3], Devriendt, J.[4], Kaviraj, S.[5], Kimm, T.[6], Peirani, S.[7]

[1]*Institute of Astronomy and Kavli Institute for Cosmology, University of Cambridge, Madingley Road, Cambridge, CB3 0HA, UK*
[2]*Institut d'Astrophysique de Paris, CNRS, Sorbonne Université, UMR7095, 98bis bd Arago, 75014 Paris, France*
[3]*Kapteyn Astronomical Institute, University of Groningen, P.O. Box 800, 9700 AV Groningen, The Netherlands*
[4] *University of Oxford, Astrophysics, Denys Wilkinson Building, Keble Road, Oxford OX1 3RH, UK*
[5] *Centre for Astrophysics Research, Department of Physics, Astronomy and Mathematics, University of Hertfordshire, Hatfield, AL10 9AB, UK*
[6] *Department of Astronomy, Yonsei University, 50 Yonsei-ro, Seodaemun-gu, Seoul 03722, Republic of Korea*
[7]*Université Côte d'Azur, Observatoire de la Côte d'Azur, CNRS, Laboratoire Lagrange, Bd de l'Observatoire,CS 34229, 06304 Nice Cedex 4, France*

Accepted XXX. Received YYY; in original form ZZZ

ABSTRACT

While it is well established that supermassive black holes (SMBHs) co-evolve with their host galaxy, it is currently less clear how lower-mass black holes, so-called intermediate-mass black holes (IMBHs), evolve within their dwarf galaxy hosts. In this paper, we present results on the evolution of a large sample of IMBHs from the NewHorizon zoom volume, which has a radius of 10 comoving **Mpc**. We show that occupation fractions of IMBHs in dwarf galaxies are at least 50 percent for galaxies with stellar masses down to 10^6 $M_\odot$, but BH growth is very limited in dwarf galaxies. In NewHorizon, IMBHs growth is somewhat more efficient at high redshift $z = 3$ but in general, IMBHs do not grow significantly until their host galaxy leaves the dwarf regime. As a result, NewHorizon under-predicts observed AGN luminosity function and AGN fractions. We show that the difficulties of IMBHs to remain attached to the centres of their host galaxies plays an important role in limiting their mass growth, and that this dynamic evolution away from galactic centres becomes stronger at lower redshift.

Key words: black hole physics – galaxies: dwarf – Methods: numerical

1 INTRODUCTION

Supermassive black holes (SMBHs) with masses of $M_{\rm BH} > 10^7 M_\odot$ or above, are well known to tightly correlate with properties of their host galaxy, such as the stellar bulge mass and the stellar velocity dispersion (see Kormendy & Ho 2013, for a review.). While these correlations are firmly established observationally for SMBHs, little data is available for black holes (BHs) in the intermediate BH mass range $10^4 < M_{\rm BH} < 10^6 M_\odot$, so-called intermediate-mass black holes (IMBHs, in the following the acronym 'BHs' refers to black holes of all masses). If extrapolations of the correlations into the intermediate-mass regime hold, such IMBHs could play the same role in dwarf galaxies that SMBHs play in massive galaxies.

IMBHs, and their potential role in shaping dwarf galaxies, is less well understood from both a simulation and an observation point of view. Observationally, the inherently lower luminosity of IMBHs due to their low BH masses make them difficult to detect and to distinguish from star formation (see Greene et al. 2019, for a review). From a theoretical point of view, the high resolution required to resolve the internal structure of simulated dwarf galaxies means they are often unresolved in large scale galaxy evolution simulations, which can therefore not be used to study the coevolution of IMBHs and their host galaxies (Haidar et al. 2022). Instead, specific simulations targeting the dwarf galaxy regime are required to study such galaxies and their central BHs.

Over the last decade, great progress has been made to expand the sample of observed IMBHs, as has been summarised in the recent reviews by Greene et al. (2019) and Mezcua (2017). There are two main methods for detecting IMBHs: kinematical studies detect BHs via the impact of their gravitational potential on host galaxy stars. This technique makes it possible to detect quiescent BHs and to directly measure the BH mass, but is limited to nearby galax-

★ E-mail: ricarda.beckmann@ast.cam.ac.uk

ies. Alternatively, IMBHs can be detected when accreting as active galactic nuclei (AGN) in a variety of wavelengths: in the optical (Molina et al. 2021; Mezcua et al. 2018; Mezcua & Sánchez 2020; Manzano-King & Canalizo 2020), the X-ray (Chilingarian et al. 2018; Latimer et al. 2021; Toptun et al. 2022), the radio (Davis et al. 2022; Yang et al. 2020; Reines et al. 2019) or the infrared (Lupi et al. 2020) to highlight a few recent studies. Other recent detection methods being explored are gamma-ray bursts potentially lensed by an IMBH (Paynter et al. 2021), short-term variability (Shin et al. 2022). In the future, gravitational wave observations will provide another opportunity to detect IMBHs (Sesana et al. 2005; Ricarte & Natarajan 2018; Bellovary et al. 2018; Amaro-Seoane 2018; Katz et al. 2020; Valiante et al. 2021; De Cun et al. 2023; Gair et al. 2011). The sample of IMBHs in dwarf galaxies is therefore very much still in the process of being assembled, and it is expected to expand significantly in coming years.

Observational surveys to date have shown that AGN fractions in dwarf galaxies are the typically observed to be in the range of $0.1-5$ percent (Latimer et al. 2021; Mezcua & Sánchez 2020; Wylezalek et al. 2018; Reines et al. 2013; Pardo et al. 2016; Aird et al. 2018; Birchall et al. 2020) but may be as high as 30 percent (Kaviraj et al. 2019; Dickey et al. 2019; Davis et al. 2022) and depend strongly on the AGN selection method (Mezcua & Sánchez 2020; Lupi et al. 2020; Greene et al. 2019) and the observational proxy for BH mass (Gallo & Sesana 2019) chosen. Firm IMBH mass detections are only available for a small sample of objects, and even fewer also have kinematics measurements of the host galaxy. For those that have both, evidence is mounting that the $M_{BH}-\sigma$ relation shows no evidence of a break in slope in the dwarf galaxy regime (Greene et al. 2019; Baldassare et al. 2020; Nguyen et al. 2019). This lack of break has been argued to be a sign that IMBHs in dwarf galaxies regulate the evolution of their host galaxy through feedback in the same way that massive galaxies are regulated by SMBHs (King & Nealon 2021). Further evidence for the theory of IMBH-regulated dwarf galaxies comes from studies of gas kinematics in dwarf that show significantly more disturbed morphologies for those with AGN than those without (Manzano-King & Canalizo 2020).

In simulations, our current picture of the co-evolution between BH and host galaxy is more mixed: some show a break in the correlations around the transition from dwarf galaxy to massive galaxy (Sharma et al. 2019; Koudmani et al. 2021), while others merely find an increase in scatter and no break (Ricarte et al. 2019; Barai & de Gouveia Dal Pino 2019; Sharma et al. 2022). As many groups find that the growth of BHs in low-mass galaxies is regulated by supernova (SN) feedback (Dubois et al. 2015; Habouzit et al. 2017; Bower et al. 2016; Anglés-Alcázar et al. 2017; Trebitsch et al. 2018), whether BHs are over-massive or under-massive in comparison to the correlation depends strongly on how both supernova feedback and BH accretion and feedback are modelled (Koudmani et al. 2022). With current SN feedback models, BH growth in dwarf galaxies is restricted mostly to high redshift (Barai & de Gouveia Dal Pino 2019; Koudmani et al. 2021) but recent evidence from simulations suggests AGN feedback in dwarf galaxies might continue to impact both star formation and galactic outflows with with strong SN feedback (Koudmani et al. 2019; Nelson et al. 2019) and that a wider variety of feedback models can lead to AGN feedback playing an even more important role in the evolution of dwarf galaxies (Koudmani et al. 2022). Analytic models also argue that the fraction of active BHs in dwarf galaxies could be higher than currenlty observed in X-ray samples (Pacucci et al. 2021). On the other hand, widespread growth of IMBHs in dwarf galaxies would lead to an overproduction of faint AGN in tension with the observed AGN luminosity function (Habouzit et al. 2017; Tillman et al. 2022).

Both observations (Mezcua & Sánchez 2020) and simulations (Bellovary et al. 2018, 2021) frequently show IMBHs in galaxies that are not located at the center of the galaxy. The discussion around the reason for this phenomenon is ongoing, but is likely linked to the evolution history of the host galaxy. Boldrini et al. (2020) use isolated halos to show that DM subhalos falling onto dwarf galaxies can displace the central IMBH by 100 pc or more, while Bellovary et al. (2021) show that the off-centre location in their sample of dwarf galaxies in a cosmological environment is due to mergers. While there generally is a large 'hidden' population of BHs in dwarf galaxies which are not sufficient active to be observable (Volonteri & Natarajan 2009), the percentage of hidden BHs that are off-centre is particularly high (Sharma et al. 2022).

In this paper, we present the sample of IMBHs in dwarf galaxies, which are here defined to have a mass of $M_{\rm dwarf} = 3{\times}10^9\ {\rm M}_\odot$, in the NewHorizon simulation[1] (Dubois et al. 2021). NewHorizon is a cosmological zoom simulation of an average density volume of the Universe that has sufficiently high resolution to resolve galaxies down to a stellar mass of $10^6{\rm M}_\odot$. We use this sample to study correlations and population statistics of IMBHs and their dwarf galaxy hosts to expand our understanding of the coevolution of massive galaxies and their BHs into the dwarf galaxy regime. The paper is structured as follows: the simulation setup is briefly recapped in Section 2. BH mass evolution is discussed in Section 3.1, BH occupation ratios are shown in Section 3.2 and mass functions are discussed in Section 3.3. The detectability of BHs is discussed in Sections 3.4 and 3.5, while the distribution of IMBHs within their host galaxies is analysed in Section 3.6. Section 4 summarises the paper.

2 SIMULATION

NewHorizon is a high-resolution resimulation of an average spherical sub-volume with a radius of 10 comoving Mpc of the Horizon-AGN simulation (Dubois et al. 2014b). NewHorizon has been presented in detail in (Dubois et al. 2021). NewHorizon was run until $z = 0.25$.

The simulation assumes a ΛCDM cosmology consistent with WMAP-7 data (Komatsu et al. 2011) with a dark energy density $\Omega_\Lambda = 0.728$, baryon density $\Omega_{\rm b} = 0.045$, total matter density $\Omega_{\rm m} = 0.272$, a Hubble constant of $H_0 = 70.4\ {\rm km\,s^{-1}\,mpc^{-1}}$, and an amplitude of the matter power spectrum and power-law index of the primordial power spectrum of $\sigma_8 = 0.81$ and $n_{\rm s} = 0.967$ respectively. A high-resolution region of radius of 10 comoving Mpc with a

[1] https://new.horizon-simulation.org/

DM mass resolution of $1.2 \times 10^6 M_\odot$ is embedded within the 142 a side comoving Mpc box of HORIZON-AGN.

All simulations within the HORIZON suite were performed using RAMSES (Teyssier 2002), using a second-order unsplit Godunov scheme for solving the Euler equations, and an HLLC Riemann solver with a MinMod Total Variation Diminishing scheme to reconstruct interpolated variables. In NEWHORIZON refinement proceeds according to a quasi-Lagrangian scheme up to a maximum resolution of 34pc at z=0, where a cell is refined if its mass exceeds 8 times the initial mass resolution. The minimum cell size is kept approximately constant throughout by adding an extra level of refinement at expansion factor $a_{\rm exp} = 0.1, 0.2, 0.4$ and 0.8. This is supplemented with a super-Lagrangian refinement criterion that enforces refinement of cells whose size is smaller than one Jeans length wherever the gas number density is larger than $5\,{\rm H\,cm^{-3}}$.

The gas follows an equation of state for an ideal monoatomic gas with an adiabatic index of $\gamma_{\rm ad} = 5/3$. Gas cooling is modelled using cooling curves from Sutherland & Dopita (1993) down to 10^4 K, assuming equilibrium chemistry. Heating from a uniform UV background takes place after redshift $z_{\rm reion} = 10$ following Haardt & Madau (1996).

Star formation occurs in cells whose hydrogen gas number density exceeds $n_0 = 10\,{\rm H\,cm^{-3}}$ following a thermo-turbulent sub-grid algorithm in combination with a Schmidt law (Kimm et al. 2017; Trebitsch et al. 2017, 2021). The stellar mass resolution is 1.3×10^4 M$_\odot$), and stars are assumed to have a Chabrier (Chabrier 2005) initial mass function with cutoffs at 0.1 and 150 M$_\odot$. Stellar feedback is modelled following Kimm et al. (2015), which separately tracks the momentum and energy conserving phase of the explosion, which reproduces the stellar-mass-to-halo-mass relation in dwarfs (Dubois et al. 2021).

New BHs are formed in any cell in which the gas and stellar density exceeds the threshold for star formation, which has a stellar velocity dispersion of more than 20 kms^{-1} and that is located more than 50 kpc from any existing BH. Each BH is formed with a mass of $M_{\rm BH,0} = 10^4$ M$_\odot$ and an initial spin of $a = 0$. We note that this is slightly below the stellar mass resolution of 1.3×10^4 M$_\odot$ which might have important consequences for how well the dynamics of BH near their seed mass is resolved in NEWHORIZON. To avoid spurious motions of BHs due to finite force resolution effects, we include an explicit drag force of the gas onto the BH, following Ostriker (1999). Two BH particles are allowed to merge into a single BH particle when they get closer than $4\Delta x$ ($\sim$ 150 pc) and when the relative velocity of the pair is smaller than the escape velocity of the binary. A detailed analysis of BH mergers in NEWHORIZON is presented in Volonteri et al. (2020).

BHs grow through un-boosted Bondi-Hoyle-Lyttleton accretion

$$\dot{M}_{\rm BHL} = \frac{4\pi (G M_{\rm BH})^2 \rho}{(c_{\rm s}^2 + v_{\rm rel}^2)^{3/2}} \quad (1)$$

where ρ, $c_{\rm s}$ and $v_{\rm rel}$ are the local mass-weighted, kernel-weighted gas density, sound speed and relative velocity between gas and BH. The accretion rate is capped at the BH's Eddington rate $\dot{M}_{\rm Edd}$, which is calculated using the spin-dependent radiative efficiency $\varepsilon_{\rm r}$:

$$\varepsilon_{\rm r} = f_{\rm att}\,(1 - E_{\rm isco}) = f_{\rm att}\left(1 - \sqrt{1 - 2/(3 r_{\rm isco})}\right) \quad (2)$$

where $r_{\rm isco} = R_{\rm isco}/R_{\rm g}$ is the radius of the innermost stable circular orbit (ISCO) in reduced units and $R_{\rm g}$ is half the Schwarzschild radius of the BH. $R_{\rm isco}$ depends on spin a. For the radio mode, the radiative efficiency used in the effective growth of the BH is attenuated by a factor $f_{\rm att} = \min(\chi/\chi_{\rm trans}, 1)$ following Benson & Babul (2009), where χ is the Eddington ratio.

During accretion, a fraction of the accreted energy is returned to the gas in one of two AGN feedback modes: 1. A quasar mode at Eddington ratios $\chi > 0.01$, in which energy is injected isotropically around the BH as thermal energy using a fixed efficiency of 15% 2. A jet mode at Eddington ratios $\chi < 0.01$, in which energy is injected as kinetic energy in bipolar jets aligned with the BH's spin axis using a spin-dependent efficiency that is higher for high spin values (see Dubois et al. 2021, for details).

BH spin is followed on-the-fly in the simulation, taking into account the angular momentum of accreted gas, BH-BH mergers and BH spindown during jet mode feedback. The BH spin model is presented in detail in Dubois et al. (2014a). When the BH is accreting with an Eddington fraction $\chi > 0.01$, BHs are either spun up or down depending on whether the angular momentum of the accreted gas feeds an aligned or misaligned sub-grid disc (King et al. 2005). For accretion at lower luminosity, the BH-driven jets are assumed to be powered by energy extraction from BH rotation (Blandford & Znajek 1977), and as a consequence the BH spin magnitude can only decrease. During mergers, the spin of the remnant is calculated according to the spin of the initial BHs, and the angular momentum of the binary, according to Rezzolla et al. (2008).

All physics included in NEWHORIZON are described in further detail in (Dubois et al. 2021). The spin evolution of black holes in NEWHORIZON is analysed in a companion publication (Beckmann et al. 2022).

2.1 Black hole and galaxy catalogue

The sample of BHs discussed in this paper includes all BHs contained within NEWHORIZON that are associated with a host galaxy from the galaxy catalogue, which in turn has to be associated with a host halo from the halo catalogue.

The DM halo catalogue consists of all un-contaminated DM halos identified by the structure-finding algorithm HOP Eisenstein & Hut (1998). A halo is considered uncontaminated if all DM particles contained within it originate from the zoom region, i.e. are at the maximum DM mass resolution.

Galaxies are identified using HOP applied to the star particles of the simulation. The galaxy consists of all galaxies flagged as level 1 (i.e. main or central structure for a given DM halo), or that have a stellar mass above 10^8M$_\odot$ if they are satellites. Galaxies are only included in the galaxy catalogue if they are located within the central 0.1 virial radii of a halo contained in the halo catalogue. The centres of galaxies and halos are identified using an iterative shrinking-sphere approach (Power et al. 2003).

To identify BHs with their host galaxy, we cycle over all

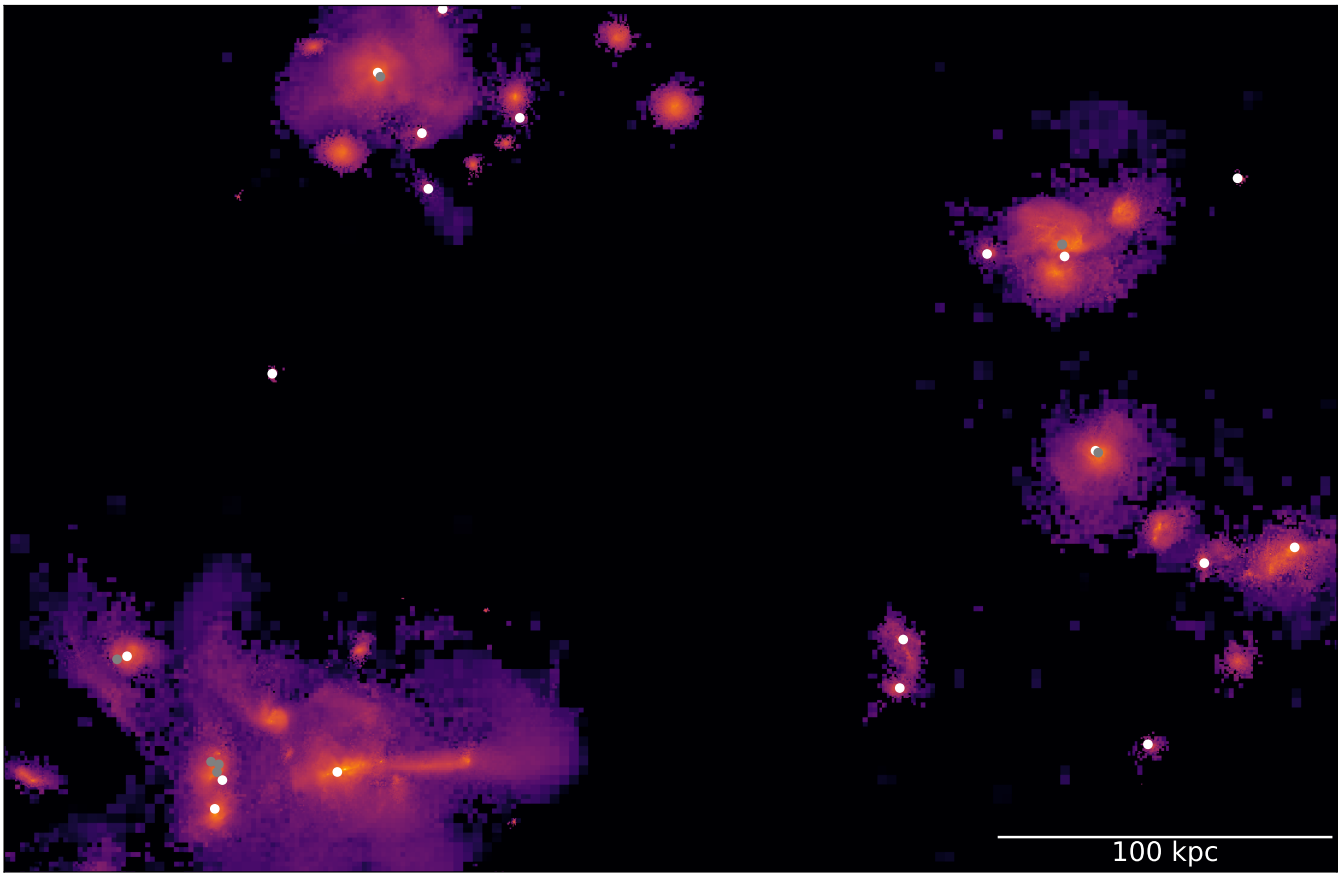

Figure 1. Stellar density projection of the central region of NewHorizon at $z = 2$. With a radius of 10 comoving Mpc for the total zoom region (equivalent to 3.3 Mpc at $z = 2$), only a small fraction of the simulated volume and sample of galaxies is shown here.

Main BHs are overplotted in white, while secondary BHs are shown in grey.

galaxies in the catalogue from most to least massive, and for each galaxy identify the most massive BH to be contained within two effective radii of the galaxy's centre. Galaxy effective radii are defined to be the geometric mean of the half-mass radius of the projected stellar densities along each of the Cartesian axis. This BH is flagged as the galaxy's main BH and removed from the sample of unallocated galaxies. We then repeat the loop over all galaxies from most to least massive, identifying all as-of-yet unallocated BHs contained within 2 effective radii of the galaxy as secondary BHs of that galaxy. A galaxy can contain multiple BHs, but a BH can only be associated with a single galaxy. The full sample of BHs discussed in this paper contains all BHs associated with host galaxies. BHs contained in contaminated galaxies and halos, and "wandering" BHs that are far from the luminous part of any galaxy are excluded from the sample. The distribution of main BH in and around galaxies for the central region of the box at $z = 2$ can be seen in Fig. 1.

3 RESULTS

3.1 Black hole - galaxy correlations

As can be seen in the top panel of Fig. 2, BHs in dwarf galaxies ($M_{\rm star} < M_{\rm dwarf} = 3 \times 10^9$ M$_\odot$) in NewHorizon grow little beyond their seed mass of 10^4 M$_\odot$ by $z = 0.25$. It is only once their host galaxy leaves the dwarf regime that main BHs grow efficiently onto the observed $M_{\rm star} - M_{\rm BH}$ correlation. Secondary BHs continue to struggle to grow beyond 10^5 M$_\odot$. As a result, the $M_{\rm BH} - M_{\rm star}$ relation shows a clear break in slope around $M_{\rm dwarf}$.

In the bottom panel of Fig. 2, we study in more detail how efficient BHs in dwarf galaxies grow over time by plotting $M_{\rm BH,acc}$, the *accreted* mass. $M_{\rm BH,acc}$ is the mass of each BH gained through gas accretion alone. It is found by taking the fiducial BH mass, $M_{\rm BH}$ and subtracting both the seed mass $M_{\rm BH,0} = 10^4$ M$_\odot$ as well as any mass gained through BH-BH mergers. As can be seen by the slope α of the linear fit to $M_{\rm BH,acc}$ vs $M_{\rm star}$ (solid lines), BHs in more massive dwarf galaxies do grow somewhat more than in low-mass dwarfs, but the slope of this trend is much shallower than for main BHs in massive galaxies. It is, however, very similar to that for secondary BHs in galaxies of all stellar masses. We caution that while the BH seed mass $M_{\rm BH,0}$ is no longer included in $M_{\rm BH,acc}$, the distribution of $M_{\rm BH,acc}$ still depend on $M_{\rm BH,0}$ as the BH accretion rate depends explicitly on the instantaneous BH mass at any given point in time (see Eq.1). If we had decided to set $M_{\rm BH,0}$ to a higher value initially, our BH would have grown faster than a BH with lower $M_{\rm BH,0}$ in the same environment.

This change in slope is different to tentative observa-

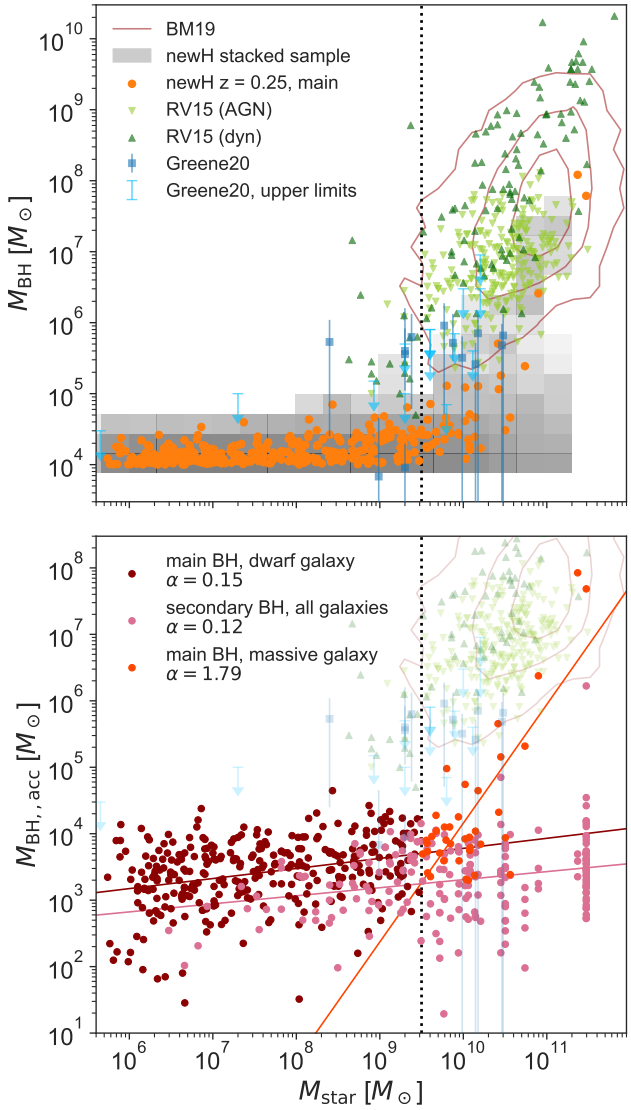

Figure 2. Correlations between mass and host galaxy properties at $z = 0.25$: [Top] Galaxy stellar mass versus BH mass M_{BH} for all main BHs. The grey distribution shows that stacked sample at all redshifts. [Bottom] Galaxy stellar mass versus accereted BH mass $M_{BH,acc}$ for all BHs. Shown on both plots for comparison are observational data from Reines & Volonteri (2015) (RV15, green triangles), Baron & Ménard (2019) (BM19, brown contours) and Greene et al. (2019) (Greene20, blue markers and limits).The same observations are shown on both panels. α denotes the slope of the fits for each population of BHs. Errorbars for RV15 are omitted for clarity. Galaxies left of the dotted black line are considered dwarf galaxies.

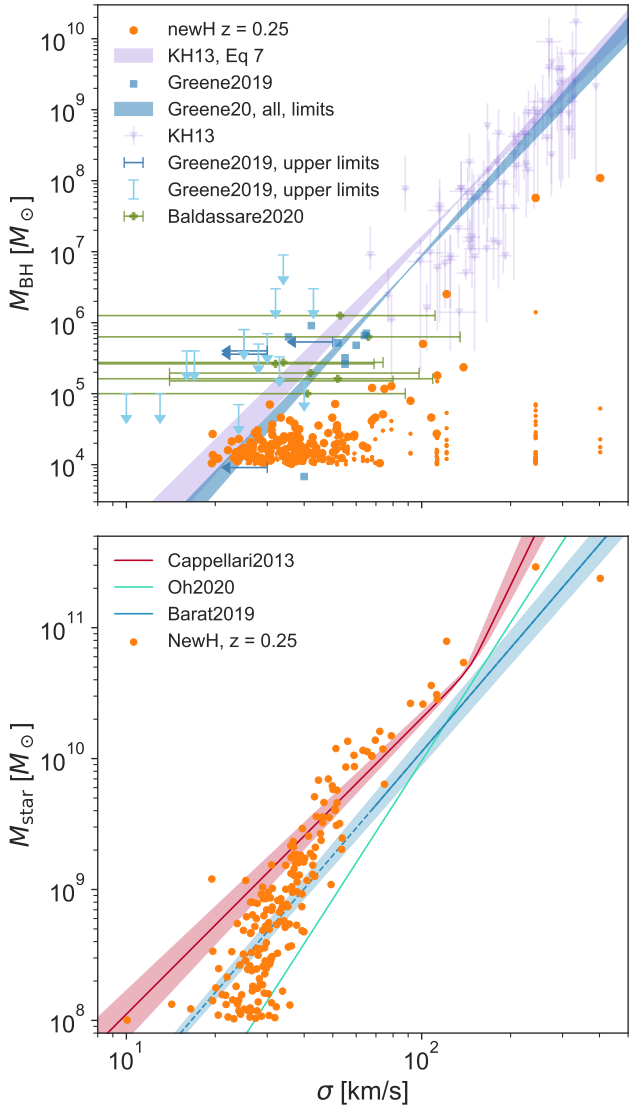

Figure 3. [Top] BH mass versus stellar velocity dispersion σ, for all galaxies with a stellar mass above $10^8 M_\odot$ at $z = 0.25$. Observations shown are from Greene et al. (2019)(Greene2019, blue markers and shaded region), Baldassare et al. (2020) (Baldassare2020, green crosses) and Kormendy & Ho (2013) (KH13, purple markers and shaded region). [Bottom] Faber-Jackson relation for redshift $z = 0.15$. Shown for comparison are observational fits from from Cappellari et al. (2013); Barat et al. (2019) and Oh et al. (2020).

tional conclusions, which show no evidence so far for a break in slope in the $M_{BH} - M_{star}$ relation during the transition from dwarf to massive galaxy (see Greene et al. 2019, for a review), and observational data points plotted for comparison in Fig. 2. The lack of change in slope could be due to an observational bias, as over-massive BHs are easier to observe for a given galaxy stellar mass than under-massive ones. No such bias exists in simulations, which could potentially skew the comparison.

Alternatively BH growth in galaxies in NewHorizon might be artificially suppressed due to an AGN feedback efficiency that could have been set too high, as the BH feedback efficiency controls the normalisation of the correlations between BH and their host galaxy properties Dubois et al. (2012). Evidence for this hypothesis comes from both the $M_{BH} - M_{star}$ relation (top panel, Fig. 2) and the $M_{BH} - \sigma$ relation (top panel, Fig 3) where BHs in NewHorizon fall consistently below observational values and fits. The bottom panel of Fig 3 confirms that this is not due to the fact that stellar velocity dispersions σ are systematically over-estimated in NewHorizon, as galaxies

at this redshift fall within observational constraints. While BHs seem to fall on the observed $M_{\rm BH}$-σ relation at the low-mass end, we caution that the mass of any BH that has not grown by at least an order of magnitude is likely to still be dominated by the numerical seed mass.

Another possible explanation for the lack of BH growth in NewHorizon is due to the position of BHs in galaxies. It is suspicious that the slope of the $M_{\rm BH,acc} - M_{\rm star}$ relation is very similar for main BH in dwarf galaxies and secondary BH in massive galaxies, which could suggest that BH in dwarf galaxies fail to grow as they are insufficiently close to the centre of their host galaxy. This effect in NewHorizon might be enhanced due to the similarity of the BH seed mass, $M_{\rm BH,0} = 10^4$ M$_\odot$, and the stellar mass resolution of 1.3×10^4 M$_\odot$, which leads to artificial scattering of BH trajectories by interactions with the stellar particles although this two-body effect is somewhat mitigated by the multi-grid gravity solver. We explore the spatial distribution of BH, and its impact on BH growth, further in Sec. 3.6.

Whether the break in the $M_{\rm BH} - M_{\rm star}$ relation is real remains an open question. With its lower seed mass of 10^4 M$_\odot$, an order of magnitude lower than previous simulations of dwarf galaxies (see e.g. Koudmani et al. 2021; Sharma et al. 2022, who used a seed mass of 10^5 M$_\odot$) and two orders of magnitude lower than the typical seed masses of 10^6 M$_\odot$ of large-scale cosmological simulations (see Haidar et al. 2022, for a comparison of different simulations), NewHorizon probes the co-evolution between IMBHs and dwarf galaxies for a larger range of galaxy masses. Using a seed mass of 10^6 M$_\odot$, Koudmani et al. (2021) find tentative evidence for a flattening of the $M_{\rm BH} - M_{\rm star}$ relation, while Sharma et al. (2022) do not, but instead discuss that this could be an artifact of their high seed mass, which artificially boosts accretion onto overmassive BHs in galaxies.

In the rest of the paper, we will explore what drives the (lack of) mass growth of BHs in dwarf galaxies, quantify whether the observable population of IMBHs in NewHorizon reproduces observed AGN in dwarf galaxies, and how the population of observable IMBHs in dwarf galaxies compares to the full sample.

3.2 Occupation fractions

One key question to understand the population of IMBHs in dwarf galaxies is how many dwarf galaxies contain a main BH. There are several ways to measure occupation fractions, as illustrated by the different panels in Fig. 4 (as a function of galaxy mass). The top panel shows the fraction of galaxies (halos) that contain at least one BH, the second panel takes BH multiplicity into account and shows the average number of BH per galaxy (halo), while the third panel denotes the fraction of galaxies that contain two or more BHs. In this section, we discuss occupation fractions of galaxies and halos which measure the presence of BHs in a given galaxy or halo, regardless of their luminosity. For the fraction of active BHs (AGN fractions), see Section 3.5.

As already seen in the $M_{\rm BH} - M_{\rm star}$ relation in Fig. 2, BHs are formed in galaxies with stellar masses as low as $M_{\rm star} = 10^6$ M$_\odot$. As can be seen in Fig. 4 occupation fractions for galaxies and halos fall with decreasing galaxy (halo) mass but remain significant across the dwarf galaxies, with

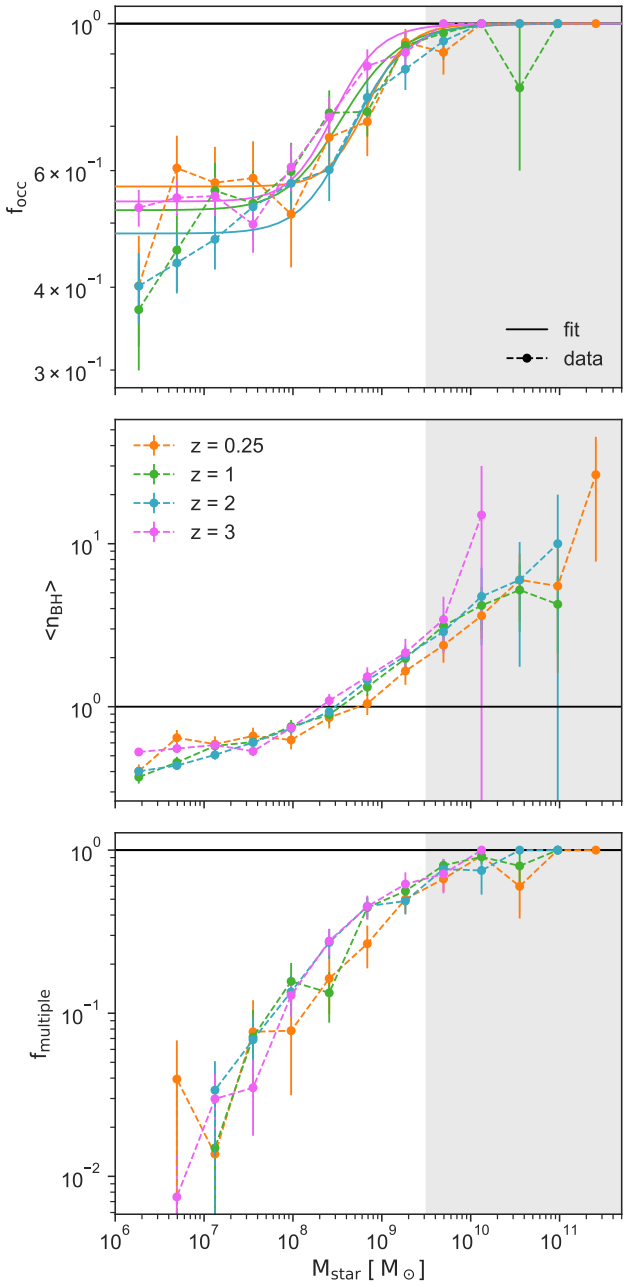

Figure 4. Fraction of galaxies that contain at least one BH [top], average number of BHs per galaxy [middle] and fraction of galaxies with multiple BHs [bottom] as a function of galaxy mass $M_{\rm star}$. A white background denotes dwarf galaxies. Solid lines on the top panel denote a fit of Eq. 3, with free parameters at each redshift listed in Table 1. Dashed lines connect data points. Error bars show Poisson errors.

even the lowest mass galaxies having a minimum occupation fraction of $f_{\rm occ} > 0.37$. There is little redshift evolution for all BHs across the mass range, with 57% of dwarf galaxies containing at least one BH at $z = 3$, in comparison to 54 % at $z = 0.25$. Multiple occupation of galaxies is fairly common for massive dwarfs (with more than 26 percent of dwarf galaxies with $M_{\rm star} > 10^8$ M$_\odot$ hosting more than one BH at $z = 0.25$), but becomes increasingly uncommon at

z	α	M'	ϵ
$z = 0.25$	0.43	8.9	39.3
$z = 1$	0.48	8.67	26.43
$z = 2$	0.52	8.78	29.49
$z = 3$	0.46	8.55	33.75

Table 1. Fitting parameters for f_{occ} from Eq. 3. Fits are shown in the top panel of Fig. 4 as solid lines.

lower galaxy stellar mass. The lack of growth of IMBHs in dwarf galaxies is therefore not due to low number statistics. NewHorizon contains 376 BHs distributed across 308 dwarf galaxies, out of a total of 552 dwarf galaxies at $z = 0.25$.

In comparison to Sharma et al. (2022), who use the Romulus25 simulation to study the population of BHs in dwarf galaxies, we also report a sharp decline in the occupation fraction with galaxy stellar mass at low redshift. At higher redshift, however, occupation fractions in NewHorizon are considerably flatter that in Romulus25. This could be due to the lower stellar mass resolution in NewHorizon (1.3×10^4 M$_\odot$) in comparison to Romulus25 ($2.1{\times}10^5$ M$_\odot$), and the corresponding lower seed mass (10^4 M$_\odot$ in NewHorizon in comparison to 10^6 M$_\odot$ for Romulus25), which allows the co-evolution of a given galaxy and its BH to be followed from earlier on in its evolution. As the intrinsic occupation fraction cannot be observed, we defer a comparison to observations to the fraction of active BHs in Section 3.5.

For ease of comparison to other datasets, the fraction of occupied galaxies has been fit with a function of the form

$$f(M) = 1 - \frac{\alpha}{1 + \left(\frac{\log(M)}{M'}\right)^{\epsilon}} \quad (3)$$

where M is the galaxy stellar mass $M_{\rm star}$, and the free parameters of the fit α, ϵ and M' are listed in Table 1 for each redshift and both galaxy samples. Similar fits for halo occupation fractions are found in Appendix A.

3.3 Black hole mass functions

One consequence of the efficient seeding and low BH growth in dwarf galaxies is that there is a large number of BHs at or near the seed mass. As a result, the BH mass function shown in Fig. 5 steepens strongly at low BH masses at all redshifts, in comparison to predictions based on observed galaxy stellar mass function (grey and black lines from Gallo & Sesana 2019 and Greene et al. 2019 respectively). Even when restricting our BH sample to more readily observable objects, by taking only main BHs of galaxies with stellar masses above 10^8M$_\odot$ into account (solid line), our BH mass functions remain very high for BHs below 10^5M$_\odot$. This is due to a combination of an efficient seeding algorithm, which creates high occupation fractions of BHs in low mass galaxies, and lack of sustained growth of the BH.

Conversely, NewHorizon under-predicts the number of more massive BHs, i.e. falls below observational limits for $M_{\rm BH} > 10^5$ M$_\odot$, suggesting that despite ample seeding, BHs struggle to grow beyond their seed masses in the environment probed here. We note that due to our comparatively small simulation volume combined with the fact that

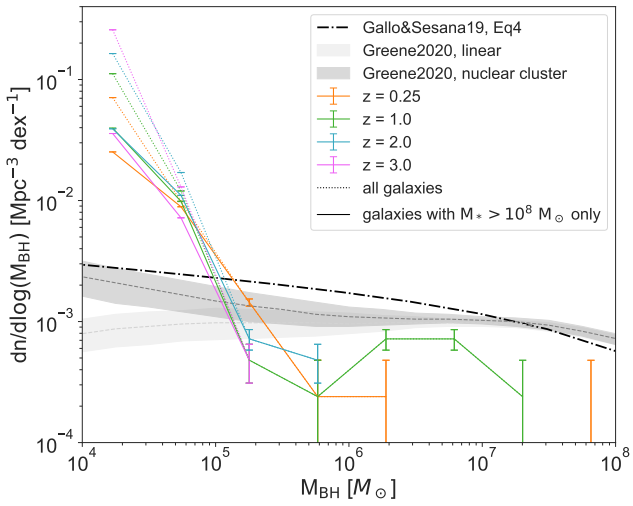

Figure 5. Evolution of the mass function of main BHs with redshift. Shown in comparison are fits based on observations from Gallo & Sesana (2019) (black dotted) and Greene et al. (2019)(grey shaded). The two models for Greene et al. (2019) are derived using a linear occupation fraction (light grey) and a nuclear cluster occupation fraction (dark grey) respectively. BH mass functions are annotated with Poisson error bars. Solid lines include main BHs of galaxies with a stellar mass above 10^8M$_\odot$, while dotted lines include all main BHs.

NewHorizon probes an average volume rather than an overdense one, number statistics for massive galaxies and their high mass BH are poor, and errorbars therefore comparatively large. We observe no clear evolution of the BH mass function with redshift for the mass bins probed at a given redshift, with the only evolution coming from BHs growing to a more massive regime over time.

3.4 Black holes in dwarf galaxies as AGN

As can be seen in Fig. 6, the ability of BHs to accrete effectively in dwarf galaxies, and the associated luminosity of AGN in dwarf galaxies, evolves strongly with redshift. In this section we differentiate between the instantaneous bolometric luminosity of a BH, $L_{\rm BH,bol}$, measured at the target redshift, a mean bolometric luminosity of a BH, $L_{\rm BH,bol,mean}$, which is calculated by taking the mean of $\log(L_{\rm BH,bol})$ for all values within $\Delta t \pm 100$ Myr around the target redshift, and a peak bolometric luminosity, $L_{\rm BH,bol,peak}$ which is defined to be the maximum luminosity of a BH within $\Delta t \pm 100$ Myr around the target redshift. We used the BH spin-based radiative efficiencies to compute the BH luminosities, as detailed in Dubois et al. (2021). As shown in the companion paper on BH spin for NewHorizon BHs (Beckmann et al. 2022), spin-based radiative efficiencies do modulate the bolometric luminosity for individual BHs by up to a factor of ~ 3, but have on average little impact on the distribution of luminosities for the whole population. This increased feedback efficiency, and consequent reduced mass growth of BHs, could explain why all main BHs in massive galaxies are found at the lower end of observations.

At high redshift, there is a wide range of accretion efficiencies across the sample of BHs. The most efficiently

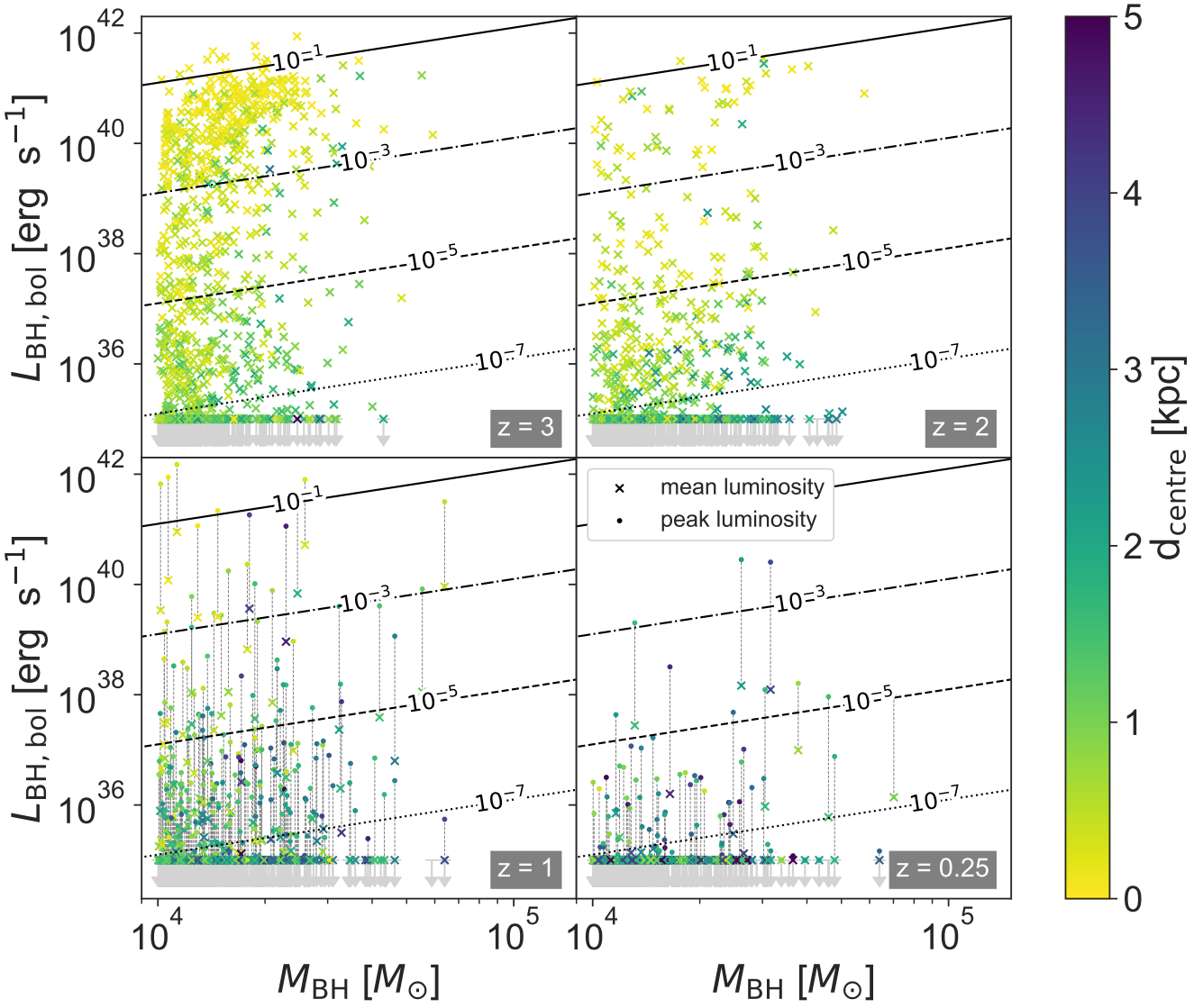

Figure 6. BH bolometric luminosity versus BH mass for all main BHs in dwarf galaxies, i.e., with stellar mass below $M_{\rm dwarf} = 3\times10^9$ M$_\odot$. Points are coloured by the distance between the BH and the centre of the host galaxy. Mean luminosities over $\pm\Delta t = 100$ Myr are shown for all redshifts (crosses), with BHs with mean $L_{\rm bol} < 10^{35}$ erg s^{-1} plotted at 10^{35} erg s^{-1} as upper limits. For $z \leq 1$, peak luminosities over the same Δt are also shown (dots). Constant Eddington fractions $f_{\rm Edd}$ are shown as black lines.

accreting BH growth with time-average Eddington ratios $f_{\rm Edd,mean} = \bar{L}_{\rm BH,bol,mean}/L_{\rm Edd} > 0.1$ but such BH are rare as the majority of the sample grow so inefficiently that their mass growth is negligible: 76.6 percent have a $f_{\rm Edd} \leq 3\times10^{-3}$, i.e. a mass growth timescale greater than the Hubble time and a luminosity far too faint to be detectable in AGN surveys. However, even among low accretors, brief accretion spikes with significantly higher luminosities are common: 23.6 percent of BHs at $z = 3$ have peak luminosities of $f_{\rm edd,peak} > 0.1$, compared to only 1.3 percent of the sample whose $f_{\rm edd,mean}$ is that high. If such accretion spikes leave a longer-lasting signal, they might enhance the observability of high-redshift BH.

With decreasing redshift, BH activity decreases markedly. At $z = 0.25$, no BH in a dwarf galaxy has a mean Eddington fraction larger than $f_{\rm Edd} = 10^{-4}$ which translates an effective minimum Salpeter time of 450 Gyr: by $z = 0.25$, growth for BHs in dwarf galaxies has effectively stopped in NewHorizon. It is well known that BH growth slows down over time (Dubois et al. 2012; Volonteri et al. 2016; Habouzit et al. 2022). However, there is growing evidence that BH growth in simulated dwarf galaxies slows down even faster than the slowdown in stellar mass growth, as similar trends to those in NewHorizon are also found in other simulations of IMBHs in dwarf galaxies, (Barai & de Gouveia Dal Pino 2019; Koudmani et al. 2021; Sharma et al. 2022), who all concluded that AGN activity in dwarf galaxies decreases strongly with redshift. A question that remains to be addressed is if, statistically, BH growth in simulated dwarf galaxies slows down faster than for more massive galaxies.

As can be seen by the colour-coding of datapoints in Fig.

6, the location of BHs plays a role in their decreased activity at low redshift: efficiently growing BHs are on average very close to the centre of their host galaxies, while the accretion efficiency of those further out drops markedly. We discuss the impact of BH location within their host galaxy further in Sec. 3.6.

Despite their low average growth rates, BHs continue to see brief bursts of activity even at low redshift, as can be seen by the peak luminosities plotted in the lower two panels of Fig. 6, which can be more than an order of magnitude higher than the mean luminosity. As a result, the bolometric luminosity functions in Fig. 7 do not drop to zero even at low redshift. At each redshift in Fig. 7, luminosities plotted are derived from a stacked sample of $L_{\rm BH,bol}$ within $\Delta t = \pm 100$ Myr of the target redshift, to account for the variation in AGN luminosity. Results do not depend sensitively on the choice of Δt. Luminosity functions are shown for both the sample of all galaxies in NewHorizon, and for dwarf galaxies only. Due to the mass evolution of galaxies over time, the two samples are indistinguishable at high redshift ($z \geq 2$) except at the very bright end, but the decrease in AGN activity for BHs in dwarf galaxies can be clearly seen at $z \leq 1$.

At high redshift, the luminosity function shows a clear peak around $10^{42}\,{\rm erg\,s^{-1}}$, which is approximately equal to the Eddington luminosity for our seed BHs. The peak in the luminosity function at this luminosity shows that many BHs at $z \geq 2$ are accreting as efficiently as permitted by our accretion algorithm (see Sec. 2 for details) One intriguing possibility is that BHs in NewHorizon are undermassive at low redshift because accretion is capped at the Eddington limit at high redshift. Even brief super-Eddington episodes could give BHs an early mass boost (Regan et al. 2018) that could influence their evolution later, although Massonneau et al. (2023) have shown that super-Eddington accretion actually reduced the overall growth of BHs in massive compact galaxies.

By $z < 1$, the peak in the luminosity function around $10^{41} - 10^{42}\,{\rm ergs^{-1}}$ has disappeared. At this redshift, the luminosity function at $L_{\rm bol} < 10^{41}\,{\rm erg\,s^{-1}}$ is still almost entirely due to BHs in dwarf galaxies, while BHs in massive galaxies dominate at higher luminosity. By $z = 0.25$, BHs in massive galaxies dominate as far down the luminosity function as $10^{37}\,{\rm erg\,s^{-1}}$, with only a small contribution from BHs in dwarf galaxies in this luminosity range due to brief peaks of AGN activity (see Fig. 6). At all redshifts, the bright end ($\rm L_{bol} > 10^{41}\,erg\,s^{-1}$) of the luminosity function is generally lower than the values by Shen et al. (2020) but in good agreement with observations by Hopkins et al. (2007), with the exception of $z = 0.25$ where NewHorizon under-predicts the luminosity function for $L < 10^{43}\,{\rm erg\,s^{-1}}$. This most likely simply reflects the fact that there are no overmassive BHs in NewHorizon and many galaxies host under-massive BHs (see Fig. 2). We note that given that NewHorizon is a zoom simulation, luminosity functions should be treated with caution as we do not have a statistically significant sample of massive galaxies, and their SMBH. As the low-luminosity end of the luminosity function could be populated by both highly accreting IMBHs and inefficiently accreting SMBHs, the absence of SMBHs in the sample will be felt across the whole luminosity function.

3.5 AGN fractions

To assess the detectability of our AGN, we also compute the X-ray luminosity of the host galaxy from both X-ray binaries (XRBs) and hot gas. For XRBs, we compute the total X-ray luminosity $L_{\rm XRB}$ by adding the contributions from soft (0.5 – 2 keV) and hard (2 – 10 keV) X-rays according to the redshift dependent relation from Lehmer et al. (2016). For X-ray emission from hot gas $L_{\rm gas}$ in the host galaxy, we compute the emission in the soft X-ray band using the relation from Mineo et al. (2012), and extrapolate to the hard X-ray band assuming a photon index of $\Lambda = 3$ following Mezcua et al. (2018). The total X-ray luminosity of the host galaxy is $L_{\rm Xray,gal} = L_{\rm XRB} + L_{\rm gas}$. A system is considered observable for a given luminosity cut $L_{\rm cut}$ if $L_{\rm Xray,BH} + L_{\rm Xray,gal} > L_{\rm cut}$, and detectable as an AGN if also $L_{\rm Xray,BH} > 2L_{\rm Xray,gal}$ following Birchall et al. (2020). The resulting distribution of $L_{\rm Xray,gal}$ versus $L_{\rm Xray,BH}$ can be seen in Fig. 8 for different redshifts.

For the BH X-ray luminosity, we calculate the 0.5 – 10 keV luminosity using the bolometric correction from Shen et al. (2020). For each galaxy, the BH X-ray luminosity $L_{\rm Xray,BH}$ is the sum of the instantaneous X-ray luminosities of all BHs associated with that galaxy, and is, hence, the sum of the galaxy's main BH as well as its secondary BHs. $L_{\rm Xray,BH}$ is therefore the BH luminosity that would be observed using a telescope with insufficient angular resolution to separate individual BHs in the galaxy. Typically, $L_{\rm Xray,BH}$ is dominated by the main BH. This is partially because not every galaxy even has a secondary BH (see the discussion on BH multiplicity in Section 3.2) and because main BHs are much more active: main BH are 2 ($z \geq 1$) to 4 ($z = 0.25$) times more likely to appear on Fig. 8, i.e. to have an instantaneous X-ray luminosity in excess of the solar luminosity $10^{34}\,{\rm erg\,s^{-1}}$ than secondary BHs. As a result, only 5 percent ($z = 0.3$) to 11 percent ($z = 0.25$) of galaxies have secondary BHs that contribute more than 20 percent to $L_{\rm Xray,BH}$.

The number of BHs that meet the Birchall et al. (2020) criterion decreases strongly with redshift: while there are plenty of BHs identifiable as AGN at $z \geq 2$, there are no BHs in dwarf galaxies at $z = 0.25$ that would be recognisable as AGN using the Birchall et al. (2020) requirement (dashed line), no matter the luminosity cut. This would remain true in even the most optimistic case if we considered the peak BH luminosity within a $\Delta t \pm 100$ Myr window around the target redshift (not shown on the plot).

As a result, the fraction of AGN in dwarf galaxies drops strongly with decreasing redshift, as can be seen in Fig. 9, from $f_{\rm AGN} \sim 17$ percent at $z = 3$ to $f_{\rm AGN} = 0$ percent at $z = 0.25$ using the instantaneous X-ray BH luminosity $L_{\rm BH,xray}$ and a luminosity cut of $L_{\rm cut} > 10^{39}\,{\rm erg\,s^{-1}}$. This is in line with previous simulation results by Barai & de Gouveia Dal Pino (2019) and Koudmani et al. (2021), who both showed that AGN activity in dwarf galaxies is significantly higher at high redshift. Like in NewHorizon, there are no remaining active BHs in dwarf galaxies in the FABLE simulations at $z \leq 0.25$ (Koudmani et al. 2021). This disagrees with observations from Birchall et al. (2020), who report an AGN fraction of 4 % at $z < 0.25$. We note that the observed AGN fractions in dwarf galaxies in literature vary strongly depending on how an AGN is defined and how the X-ray luminosity of the host galaxy is accounted for. As a result, some X-ray surveys find values as high as 30 percent (Zhang et al. 2009;

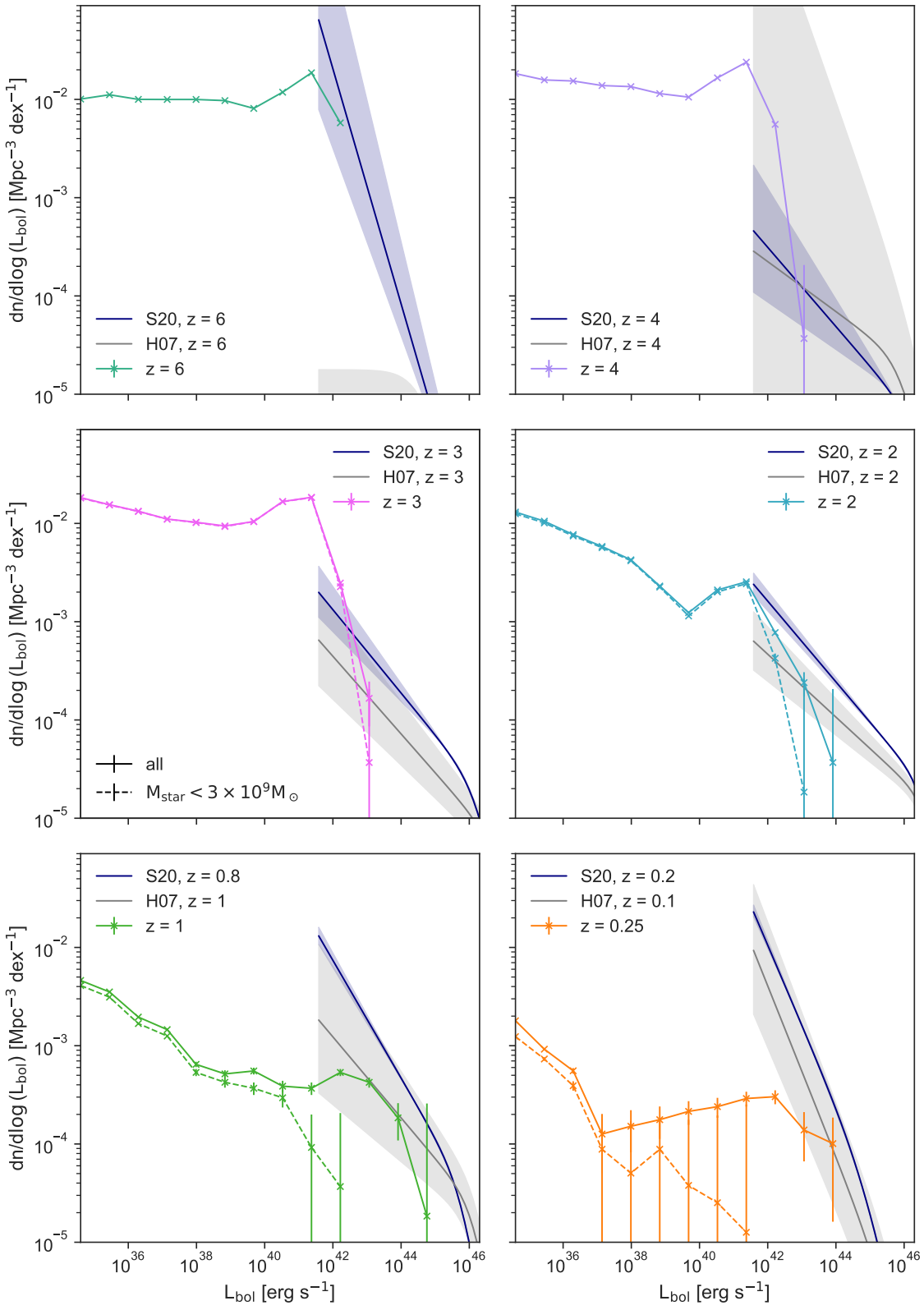

Figure 7. Bolometric BH luminosity functions with Poisson error bars for the full sample of galaxies (solid) and dwarf galaxies (dashed). At $z > 3$, all galaxies are dwarf galaxies so only one line is shown for clarity. Luminosities shown are derived from a stacked sample within ±100 Myr of the target redshift. Shaded regions show fits to observational luminosity functions by Hopkins et al. (2007) (H07) and Shen et al. (2020) (S20) for comparison.

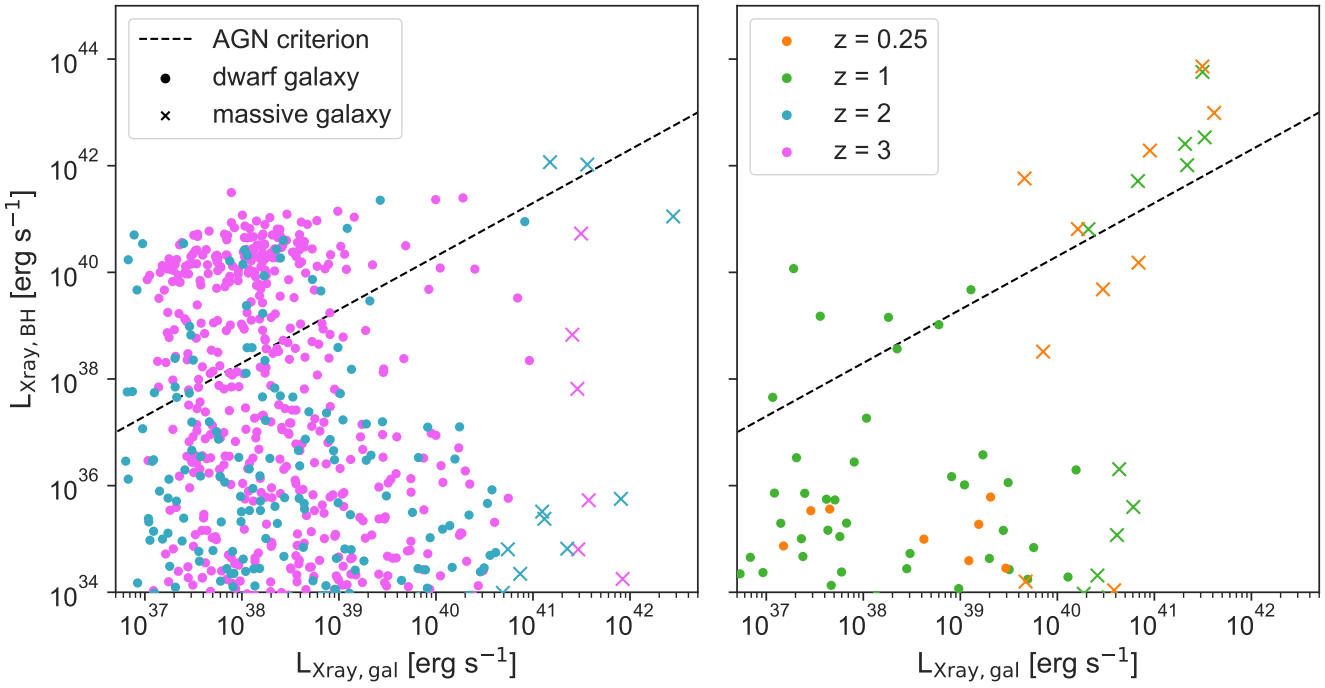

Figure 8. Distribution of X-ray luminosity of BHs versus that of their host galaxies using the mean BH luminosity (left $z = 3\&2$, right $z = 1\&0.25$). Data-points above the dashed line are detectable as AGN, as they have $L_{\rm Xray,BH} > 2L_{\rm Xray,gal}$, if the combined luminosity of BH and galaxy exceeds the luminosity cut, i.e. if also $L_{\rm Xray,BH} + L_{\rm Xray,gal} > L_{\rm cut}$ for a given $L_{\rm cut}$.

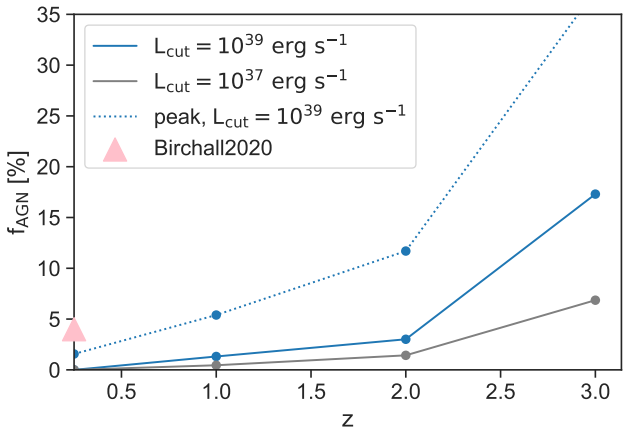

Figure 9. Fraction of observable AGN as a function of redshift for all dwarf galaxies with a total X-ray luminosity above 10^{39} erg s^{-1} (blue) and 10^{37} erg s^{-1} (grey). Solid lines use the instantaneous $L_{\rm xray,BH}$, while dotted lines use the peak $L_{\rm xray,BH}$ within $\Delta t \pm 100$ Myr. Coloured markers show observational data measured at $z < 0.25$ by Birchall et al. (2020), for luminosity cuts of $> 10^{39}$ erg s^{-1}.

She et al. 2017). Here we restrict the comparison to Birchall et al. (2020) as we have designed our AGN observability criteria to reflect theirs.

AGN fractions depend strongly on the luminosity cut, as can be seen by comparing the 10^{39} ergs^{-1} to the even more optimistic 10^{37} ergs^{-1}, which shows lower $f_{\rm AGN}$ at all redshifts probed here. This is due to the fact that with increasing luminosity cut, the number of AGN in the sample increases but the number of galaxies increases even faster. A direct comparison to observations of this redshift evolution is difficult as observing AGN with luminosity cuts as low as 10^{39} erg s^{-1}, let alone the lower cut of 10^{37} erg s^{-1}, is currently only possible at very low redshift. Instead, observations of the redshift evolution of $f_{\rm AGN}$ such as those presented in Mezcua et al. (2018) use luminosity cuts of the order of $10^{40.5}$ erg s^{-1}, which no BH in dwarf galaxies achieve in NewHorizon, even at $z = 3$. At such higher luminosity cuts, observations show a predominantly flat evolution of the AGN fraction with decreasing redshift at $z < 1$ (Mezcua et al. 2018; Birchall et al. 2020), which suggests that current simulations over-quench AGN. This hypothesis is further supported by the fact that there are no bright AGN at all in NewHorizon. This conclusion assumes that AGN are observed at their instantaneous luminosity at $z = 0.25$. If we make the generous assumption that AGN activity leaves an observable signal that persists for longer than the AGN outburst itself, and that we can therefore observe AGN at their peak activity within a $\Delta t = 100$ Myr window (similar to the analysis in Fig. 7) then two potential AGN do appear in the sample at $z = 0.25$. This raises the observable AGN fraction to $f_{\rm AGN} = 1.5\%$. Despite this being a generous assumption, the resulting AGN fraction still lies below the observed fraction of 4 % by Birchall et al. (2020). We also caution that this assumes that the observable AGN signal does not fade at all for up 100 Myr after the outburst has ended, and therefore represents an upper limit.

Overall, we conclude that mass growth for BH with seed

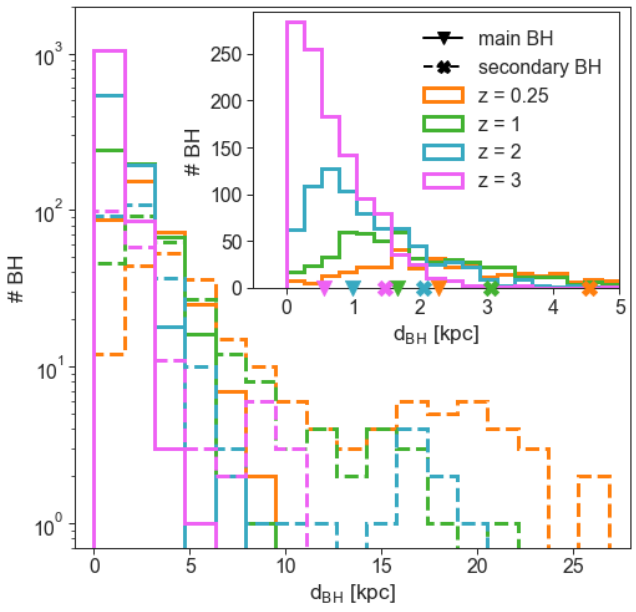

Figure 10. Distribution of the distance between BHs and the centre of their host galaxies, $d_{\rm BH}$ for main (solid) and secondary (dashed) BHs. The in-set pan shows a zoom in on the range $d_{\rm BH} < 5$ kpc and the median distance of main (secondary) BHs as triangles (crosses) at each redshift.

masses of 10^4 M$_\odot$ in NewHorizon is stifled below observed limits, particularly at low redshift. The time window for efficient BH growth is too short for BHs to compensate for the lack of earlier growth at the seed mass. This could suggests that BHs seeds in dwarf galaxies are formed as massive seed BHs ($> 10^4$ M$_\odot$), or that current SN prescriptions are too strong to allow for the observed BH growth. Other potential numerical effects, besides SN prescriptions, that might lead to the observed over-quenching, is an overestimated AGN feedback efficiency. However, it is not as simple as simply decreasing the SN feedback strength, as doing so will over-predict the stellar-to-halo mass relation, which for NewHorizon is already at the upper end of empirical constraints. Instead, it might be more a question of where SN energy is deposited, how turbulence is injected in the interstellar medium and how SN and possibly AGN feedback can continue to regulate the galaxy mass content without over-quenching IMBHs in dwarf galaxies (see Koudmani et al. 2022, for a detailed investigation of the impact of SN feedback strength on IMBH growth in dwarf galaxies). Alternatively, the lack of BH growth could be a sign of other relevant missing physics, such as the suppression of cooling from cosmic rays which have been shown to suppress the star formation rate (SFR), and resulting SN injection rate, by a factor of 2-3 (Dashyan & Dubois 2020).

3.6 Distribution of black holes in dwarf galaxies

To grow efficiently, BHs must be able to tap into an abundant local supply of cold gas. The lack of growth for BHs in NewHorizon could therefore be due to one of two reasons: either dwarf galaxies in NewHorizon are cold gas poor, or BHs are not located where the cold gas is. As can be seen by

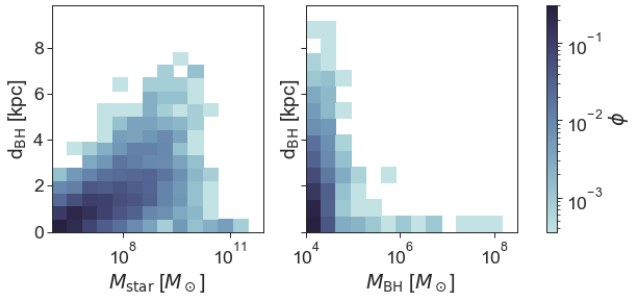

Figure 11. Log-normalised distribution ϕ of the distance between main BHs and the centre of their host galaxies, $d_{\rm BH}$ as a function of the host galaxy mass $M_{\rm star}$ (left) and BH mass $M_{\rm BH}$ (right) for a stacked sample of all BHs at $z = 3, 2, 1$ and 0.25.

the colour-coding of datapoints in Fig. 6, the location of BHs certainly plays a role in their decreased activity: efficiently growing BHs are on average very close to the centre of their host galaxies, while the ability to accrete of those further out drops markedly. The distribution of BHs from the centre of their host galaxy evolves with redshift, as can be seen qualitatively in Fig. 6 and more quantitatively in Fig. 10. The sample of BHs plotted in Fig. 10 separately analyses the distribution of main and secondary BHs, unlike Fig. 8 which only shows main BHs. At all redshifts, main BHs dominate the sample, with 86% of BHs at $z = 3$ classified as 'main' which decreases to 62% at $z = 0.25$.

In general, main BHs are closer to the centre of their host galaxy than secondary BHs, as can be seen in Fig. 10. We note that main BHs being closer to the centre of their host galaxy is not by design as the 'main' BH of a galaxy is not selected to be the one located closest to the centre of the galaxy. Instead, it is defined to be the most massive BH that meets the criterion of being identified with a given galaxy (see Sec. 2.1 for more details).

Both main BHs and secondary BHs become less centrally located over time. The median distance of BHs to the centre of their galaxy increases from 0.68 kpc at $z = 3$ to 2.96 kpc at $z = 0.25$ for main BHs, and from 1.48 kpc at $z = 3$ to 4.55 kpc at $z = 0.25$ for secondary BHs. This increase in separation between galaxy centre and BH for both main and secondary BH is partially due to the increased size of galaxies at low redshift but not exclusively. Accounting for the increase in average galaxy size, here measured by the galaxies' effective radius $r_{\rm eff}$ with decreasing redshift, the median distance still increases from $1.0r_{\rm eff}$ at $z = 3$ to $1.3r_{\rm eff}$ at $z = 0.25$ for main BHs. We therefore conclude that main BHs struggle to remain attached to the centre of their host galaxy for long periods of time, and both main and secondary BH become less central over time. As will be discussed in detail in a companion publication entirely focused on the dynamics of BHs in NewHorizon Beckmann et al. (2023), BHs predominantly become displaced from their galactic center during galaxy mergers. Dynamical timescales for such low mass BHs are extremely long, BHs struggle to settle back into galactic centers following such disturbances.

As can be seen in Fig. 11 it is predominantly low-mass BHs in low-mass galaxies which struggle to remain attached to the centre. While BHs close to the centre of their host

galaxy exist at all BH and galaxy masses, it is only above a threshold BH mass ($M_{\rm BH} \gtrsim 10^5$ M$_\odot$) and a threshold host galaxy mass ($M_{\rm star} \gtrsim 10^{10}$ M$_\odot$) that main BH can be reliably found in the centre of the galaxy.

From previous work, BHs in galaxies that are not located in the centre of galaxies is not unexpected. Bellovary et al. (2021) found that BHs in dwarf galaxies are frequently displaced from the centre of their host galaxy following galaxy mergers, and Sharma et al. (2022) report that a significant fraction of their BHs in dwarf galaxies are off-centre. Observationally, there is also evidence for the fact that BHs in dwarf galaxies wander. Observationally, Reines et al. (2019) reported that the majority of their radio-selected AGN in dwarf galaxies are off-centre with respect to the host galaxy. Part of this is due to the fact that dwarf galaxies frequently show disturbed morphologies, so there is no clear 'centre' for BHs to be located in. However, the displacement of BHs in dwarf galaxies goes beyond this effect, as the fraction of disturbed morphologies in dwarf galaxies falls with decreasing redshift (in NewHorizon, from 20 percent at $z = 3$ to 5 percent at $z = 1$, see Martin et al. 2020), while the mean distance of main and secondary BHs to the centre of the galaxy increases with decreasing redshift.

By $z = 0.25$, only 27 percent of main BHs (and 30 percent of all BHs) remain within 1 kpc of the centre, which is lower than in previous studies of BHs in dwarf galaxies such as Sharma et al. (2022). This is through a mix of BHs being displaced by galaxy mergers (Bellovary et al. 2021) but most likely also a consequence of NewHorizon lower BH seed mass, as dynamical timescales for BHs to settle back to galactic centres is directly proportional to the mass of the BH (Pfister et al. 2019), and lower-mass BHs struggle more than higher mass BHs to sink back to the centre (Ma et al. 2021; Bellovary et al. 2021) (see also Fig. 11). In NewHorizon, BH might additionally be prone to wandering as their seed mass of $M_{\rm BH,0} = 10^4$ M$_\odot$ is close to the stellar mass resolution of 1.3×10^4 M$_\odot$ of NewHorizon, which induces stochastic effects in their orbits. Additionally, we do not analytically model the unresolved dynamical friction from star and DM particles, which has been shown to play a strong role in allowing BHs to sink to the centre of galaxies (Pfister et al. 2019; Chen et al. 2021), and the dynamical friction from gas becomes less efficient at increased resolution due to instabilities in the wake (Beckmann et al. 2018) and the turbulent nature of the gas (Lescaudron et al. 2022).

3.7 Discussion

One of the clear take-aways of the results presented here is how strongly observational signatures of IMBHs at low redshift are influenced by the BH dynamics, which has significant consequences on both the $M_{\rm BH} - M_{\rm star}$ and observability of IMBHs at low redshift. As can be seen in Fig. 7, the radial distance of BHs from the centre of their host galaxy is anti-correlated with the accretion efficiency, and therefore regulates the long-term mass evolution: In NewHorizon , BHs struggle to grow until the gain masses of $\sim 5 \times 10^5$ M$_\odot$, at which point BHs sink efficiently to the centre of galaxies (see Fig. 11) and grow onto the observed correlations (see Fig. 2). This causes a clear break in the $M_{\rm BH} - M_{\rm star}$ relation, which is not reported in other works on IMBHs in dwarf galaxies that either force the BH to remain attached to the centres of galaxies (Barai & de Gouveia Dal Pino 2019), or do not study the low-mass regime by using a high seed masses (e.g. Sharma et al. 2022, who use a seed mass of 10^6 M$_\odot$). Both works note that their lack of dynamics and high seed mass respectively mean their results are likely an upper limit on IMBH growth in dwarf galaxies. By the same argument, the wandering of BHs in NewHorizon means our results likely present a lower limit on the growth of IMBHs in dwarf galaxies. In this context it is interesting to note that Koudmani et al. (2019), who use a lower seed mass of 10^5 M$_\odot$ as well as a repositioning scheme also report some evidence for flattening of the $M_{\rm BH} - M_{\rm star}$ relation. Like NewHorizon, they also under-predict observed X-ray AGN fractions at low redshift (see Fig. 9), despite the repositioning scheme that forces their IMBHs into galactic centres. Overall this shows that IMBHs in dwarf galaxies are extremely sensitive probes of BH and galaxy coevolution, and that the dynamics of the BHs lie at the heart of when and how IMBHs and dwarf galaxies coevolve.

This points to a big open problem in the field: if low-mass BHs struggle to remain attached to the centres of galaxies, and not being attached to the centres of galaxies means BHs struggle to grow, how can we explain the observed, active IMBHs in dwarf galaxies? Either there is something that is fundamentally missing in our understanding (or numerical modelling) of BH dynamics, or all seed BHs must be sufficiently massive to avoid such dynamical difficulties. We will further explore the dynamics of both main and secondary BHs in NewHorizon galaxies, and its impact on long-term IMBH mass growth, in detail in an upcoming companion paper Beckmann et al. (2023).

4 CONCLUSIONS

In this paper we studied the evolution of BHs in dwarf galaxies in the NewHorizon large-volume zoom simulation. We found that

(i) BHs do not start growing efficiently until their host galaxy leaves the dwarf galaxy regime (i.e. when $M_{\rm star} > 3 \times 10^9$ M$_\odot$. As a result, most BHs in dwarf galaxies remain near their seed mass for long periods of time (here $M_{\rm BH,0} = 10^4$ M$_\odot$. There is a weak trend for BHs in more massive dwarf galaxies to grow more through accretion than in low-mass dwarfs.

(ii) Occupation fractions of BHs in dwarf galaxies remain high and show little evolution with redshift. The fraction of galaxies hosting multiple BHs increases strongly with host galaxy stellar mass and reaches unity as galaxies become massive.

(iii) BHs grow much more actively at high redshift ($z \geq 2$), where there are a significant number of objects that have time-averaged high Eddington ratios. At low redshift (≤ 1, average Eddington ratios fall very low but brief bursts of higher activity remain common. These bursts are too infrequent to contribute significant mass growth to the BH, but do make BHs intermittently observable.

(iv) When looking at the X-ray luminosity of BHs and their host galaxies, most BHs are insufficiently luminous to outshine their host even at high redshift. This means that

even at high redshift ($z = 3$), the fraction of dwarf galaxies that host an AGN that can be detected above an optimistic luminosity threshold of 10^{39} ergs^{-1} is only ~ 17 percent.

(v) At lower redshift, the fraction of AGN for a given X-ray luminosity cut decreases, with no observable AGN remaining at $z \sim 0.25$.

(vi) Due to their low seed mass, BHs in NewHorizon struggle to remain attached to the centres of their host galaxies, with the average distance between BHs and galaxy centre increasing from 0.68 kpc at $z = 3$ to 2.96 kpc at $z = 0.25$. BHs in massive galaxies sink efficiently to the centre.

Overall, the evolution of the BH population in NewHorizon shows that the lower seed mass exacerbates many of the processes that limit BH growth. Previous simulation work with higher seed mass should consequently be seen as an upper limit to how much BHs in dwarf galaxies can grow given our current model of BH dynamics, BH accretion and SN feedback. As such, dwarf galaxies remain a promising laboratory to constrain stellar feedback and BH physics.

DATA AVAILABILITY

All data used in this paper is available upon request to the first author.

ACKNOWLEDGEMENTS

This work was granted access to the HPC resources of CINES under the allocations c2016047637, A0020407637 and A0070402192 by Genci, KSC-2017-G2-0003 by KISTI, and as a "Grand Challenge" project granted by GENCI on the AMD Rome extension of the Joliot Curie supercomputer at TGCC. This research is part of the Spin(e) ANR-13-BS05-0005 (http://cosmicorigin.org), Segal ANR-19-CE31-0017 (http://secular-evolution.org) and Horizon-UK projects. This work has made use of the Infinity cluster on which the simulation was post-processed, hosted by the Institut d'Astrophysique de Paris. RSB would like to thank Newnham College, Cambridge, for financial support. TK was supported by the National Research Foundation of Korea (NRF) grant funded by the Korea government (No. 2020R1C1C1007079 and No. 2022R1A6A1A03053472). We warmly thank S. Rouberol for running it smoothly. The large data transfer was supported by KREONET which is managed and operated by KISTI. RSB gratefully acknowledges funding from Newnham College, Cambridge. SK acknowledges support from the STFC [ST/S00615X/1] and a Senior Research Fellowship from Worcester College, Oxford.

REFERENCES

Aird J., Coil A. L., Georgakakis A., 2018, MNRAS, 474, 1225
Amaro-Seoane P., 2018, Phys. Rev. D, 98, 063018
Anglés-Alcázar D., Faucher-Giguère C.-A., Quataert E., Hopkins P. F., Feldmann R., Torrey P., Wetzel A., Kereš D., 2017, MNRAS, 472, L109
Baldassare V. F., Dickey C., Geha M., Reines A. E., 2020, ApJ, 898, L3
Barai P., de Gouveia Dal Pino E. M., 2019, MNRAS, 487, 5549
Barat D., et al., 2019, MNRAS, 487, 2924
Baron D., Ménard B., 2019, MNRAS, 487, 3404
Beckmann R. S., Slyz A., Devriendt J., 2018, MNRAS, 478, 995
Beckmann R. S., Dubois Y., Volonteri M., 2022, in prep
Beckmann R. S., Volonteri M., Dubois Y., 2023, in prep
Bellovary J., Cleary C., Munshi F., Tremmel M., Christensen C., Brooks A., Quinn T., 2018, MNRAS, 482, 2913
Bellovary J. M., et al., 2021, MNRAS, 505, 5129
Benson A. J., Babul A., 2009, MNRAS, 397, 1302
Birchall K. L., Watson M. G., Aird J., 2020, MNRAS, 492, 2268
Blandford R. D., Znajek R. L., 1977, MNRAS, 179, 433
Boldrini P., Mohayaee R., Silk J., 2020, MNRAS, 495, L12
Bower R., Schaye J., Frenk C. S., Theuns T., Schaller M., Crain R. A., McAlpine S., 2016, MNRAS, 465, 32
Cappellari M., et al., 2013, MNRAS, 432, 1862
Chabrier G., 2005, The Initial Mass Function: From Salpeter 1955 to 2005. Vol. 327, Springer Netherlands, doi:10.1007/978-1-4020-3407-7_5, http://link.springer.com/10.1007/978-1-4020-3407-7_5
Chen N., Ni Y., Tremmel M., Matteo T. D., Bird S., DeGraf C., Feng Y., 2021, MNRAS, 510, 531
Chilingarian I. V., Katkov I. Y., Zolotukhin I. Y., Grishin K. A., Beletsky Y., Boutsia K., Osip D. J., 2018, ApJ, 863, 1
Dashyan G., Dubois Y., 2020, A&A, 638, A123
Davis F., et al., 2022, MNRAS, 511, 4109
De Cun V. I., Bellovary J. M., Katz M. L., 2023, MNRAS, 520, 3916
Dickey C. M., Geha M., Wetzel A., El-Badry K., 2019, ApJ, 884, 180
Dubois Y., Devriendt J., Slyz A., Teyssier R., 2012, MNRAS, 420, 2662
Dubois Y., Volonteri M., Silk J., Devriendt J., Slyz A., 2014a, MNRAS, 440, 2333
Dubois Y., et al., 2014b, MNRAS, 444, 1453
Dubois Y., Volonteri M., Silk J., Devriendt J., Slyz A., Teyssier R., 2015, MNRAS, 452, 1502
Dubois Y., et al., 2021, A&A, 651, A109
Eisenstein D. J., Hut P., 1998, ApJ, 498, 137
Gair J. R., Mandel I., Miller M. C., Volonteri M., 2011, Gen. Relativ. Gravit., 43, 485
Gallo E., Sesana A., 2019, ApJ, 883, L18
Greene J. E., Strader J., Ho L. C., 2019, ARA&A, 58, 257
Haardt F., Madau P., 1996, ApJ, 461, 20
Habouzit M. M., Volonteri M., Dubois Y., 2017, MNRAS, 468, 3935
Habouzit M., et al., 2022, MNRAS, 509, 3015
Haidar H., et al., 2022, MNRAS, 514, 4912
Hopkins P. F., Richards G. T., Hernquist L., 2007, ApJ, 654, 731
Katz M. L., Kelley L. Z., Dosopoulou F., Berry S., Blecha L., Larson S. L., 2020, MNRAS, 491, 2301
Kaviraj S., Martin G., Silk J., 2019, MNRAS, 489, L12
Kimm T., Cen R., Devriendt J., Dubois Y., Slyz A., 2015, MNRAS, 451, 2900
Kimm T., Katz H., Haehnelt M., Rosdahl J., Devriendt J., Slyz A., 2017, MNRAS, 466, stx052
King A., Nealon R., 2021, MNRAS, 502, L1
King A. R., Lubow S. H., Ogilvie G. I., Pringle J. E., 2005, MNRAS, 363, 49
Komatsu E., et al., 2011, ApJSupplement Series, 192, 18
Kormendy J., Ho L. C., 2013, ARA&A, 51, 511
Koudmani S., Sijacki D., Bourne M. A., Smith M. C., 2019, MNRAS, 484, 2047
Koudmani S., Henden N. A., Sijacki D., 2021, MNRAS, 503, 3568
Koudmani S., Sijacki D., Smith M. C., 2022, MNRAS, 516, 2112
Latimer C. J., Reines A. E., Bogdan A., Kraft R., 2021, ApJ, 922, L40
Lehmer B. D., et al., 2016, ApJ, 825, 7

Lescaudron S., Dubois Y., Beckmann R. S., Volonteri M., 2022, Accepted in A&A, p. arXiv:2209.13548
Lupi A., Sbarrato T., Carniani S., 2020, MNRAS, 492, 2528
Ma L., Hopkins P. F., Ma X., Anglés-Alcázar D., Faucher-Giguère C.-A., Kelley L. Z., 2021, MNRAS, 508, 1973
Manzano-King C. M., Canalizo G., 2020, MNRAS, 498, 4562
Martin G., et al., 2020, MNRAS, 500, 4937
Massonneau W., Volonteri M., Dubois Y., Beckmann R. S., 2023, A&A, 670, A180
Mezcua M., 2017, Int. J. Mod. Phys. D, 26, 1730021
Mezcua M., Sánchez H. D., 2020, ApJ, 898, L30
Mezcua M., Civano F., Marchesi S., Suh H., Fabbiano G., Volonteri M., 2018, MNRAS, 478, 2576
Mineo S., Gilfanov M., Sunyaev R., 2012, MNRAS, 426, 1870
Molina M., Reines A. E., Latimer C. J., Baldassare V., Salehirad S., 2021, ApJ, 922, 155
Nelson D., et al., 2019, MNRAS, 490, 3234
Nguyen D. D., et al., 2019, ApJ, 872, 104
Oh S., et al., 2020, MNRAS, 495, 4638
Ostriker E. C., 1999, ApJ, 513, 252
Pacucci F., Mezcua M., Regan J. A., 2021, ApJ, 920, 134
Pardo K., et al., 2016, ApJ, 831, 203
Paynter J., Webster R., Thrane E., 2021, Nat. Astron, 5, 560
Pfister H., Volonteri M., Dubois Y., Dotti M., Colpi M., 2019, MNRAS, 486, 101
Power C., Navarro J. F., Jenkins A., Frenk C. S., White S. D. M., Springel V., Stadel J., Quinn T., 2003, MNRAS, 338, 14
Regan J. A., Downes T. P., Volonteri M., Beckmann R., Lupi A., Trebitsch M., Dubois Y., 2018, MNRAS, 486
Reines A. E., Volonteri M., 2015, ApJ, 813, 82
Reines A. E., Greene J. E., Geha M., 2013, ApJ, 775, 116
Reines A., Condon J., Darling J., Greene J., 2019, ApJ, 888, 36
Rezzolla L., Barausse E., Dorband E. N., Pollney D., Reisswig C., Seiler J., Husa S., 2008, Phys. Rev. D, 78, 044002
Ricarte A., Natarajan P., 2018, MNRAS, 481, 3278
Ricarte A., Tremmel M., Natarajan P., Quinn T., 2019, MNRAS, 489, 802
Sesana A., Haardt F., Madau P., Volonteri M., 2005, ApJ, 623, 23
Sharma R. S., Brooks A. M., Somerville R. S., Tremmel M., Bellovary J., Wright A. C., Quinn T. R., 2019, ApJ, 897, 103
Sharma R. S., Brooks A. M., Tremmel M., Bellovary J., Ricarte A., Quinn T. R., 2022, ApJ, 936, 82
She R., Ho L. C., Feng H., 2017, ApJ, 835, 223
Shen X., Hopkins P. F., Faucher-Giguère C.-A., Alexander D. M., Richards G. T., Ross N. P., Hickox R. C., 2020, MNRAS, 495, 3252
Shin L., Woo J.-H., Son D., Cho H., Kim T., Gallo E., Kang W., 2022, AJ, 163, 73
Sutherland R. S., Dopita M. A., 1993, ApJSupplement Series, 88, 253
Teyssier R., 2002, doi:10.1051/0004-6361:20011817, 385, 337
Tillman M. T., Wellons S., Faucher-Giguère C.-A., Kelley L. Z., Anglés-Alcázar D., 2022, MNRAS, 511, 5756
Toptun V., Chilingarian I., Grishin K., Katkov I., Zolotukhin I., Goradzhanov V., Demianenko M., Kuzmun I., 2022. Crossref, pp 304–306, doi:10.51194/VAK2021.2022.1.1.117, http://www.inasan.ru/wp-content/uploads/2022/02/VAK_2021_.pdf#page=305
Trebitsch M., Blaizot J., Rosdahl J., Devriendt J., Slyz A., 2017, MNRAS, 470, 224
Trebitsch M., Volonteri M., Dubois Y., Madau P., 2018, MNRAS, 478, 5607
Trebitsch M., et al., 2021, A&A, 653, A154
Valiante R., et al., 2021, MNRAS, 500, 4095
Volonteri M., Natarajan P., 2009, MNRAS, 400, 1911
Volonteri M., Dubois Y., Pichon C., Devriendt J., 2016, MNRAS, 460, 2979
Volonteri M., et al., 2020, MNRAS, 498, 2219
Wylezalek D., Zakamska N. L., Greene J. E., Riffel R. A., Drory N., Andrews B. H., Merloni A., Thomas D., 2018, MNRAS, 474, 1499
Yang J., Gurvits L. I., Paragi Z., Frey S., Conway J. E., Liu X., Cui L., 2020, MNRAS, 495, L71
Zhang W. M., Soria R., Zhang S. N., Swartz D. A., Liu J., 2009, ApJ, 699, 281

z	α	M'	ϵ
$z = 0.25$	0.93	9.65	9.98
$z = 1$	0.61	10.36	28.45
$z = 2$	0.67	10.31	21.25
$z = 3$	0.48	10.5	36.2

Table A1. Fitting parameters for f_{occ} from Eq. 3 as a function of halo mass M_{halo}. Fits are shown in the top panel of Fig. A1 as solid lines.

APPENDIX A: HALO OCCUPATION FRACTIONS

Fig. A1 shows the halo occupation fraction and the average number of BHs per halo. The analysis shown here is equivalent to that for galaxies in Section 3.2, but as a function of DM halo mass rather than galaxy stellar mass. As before, occupation fractions are fit with a function of the form of Eq. 3 where M is now the DM halo mass M_{halo}, with fitting parameters shown in Tab. A1.

This paper has been typeset from a TEX/LATEX file prepared by the author.

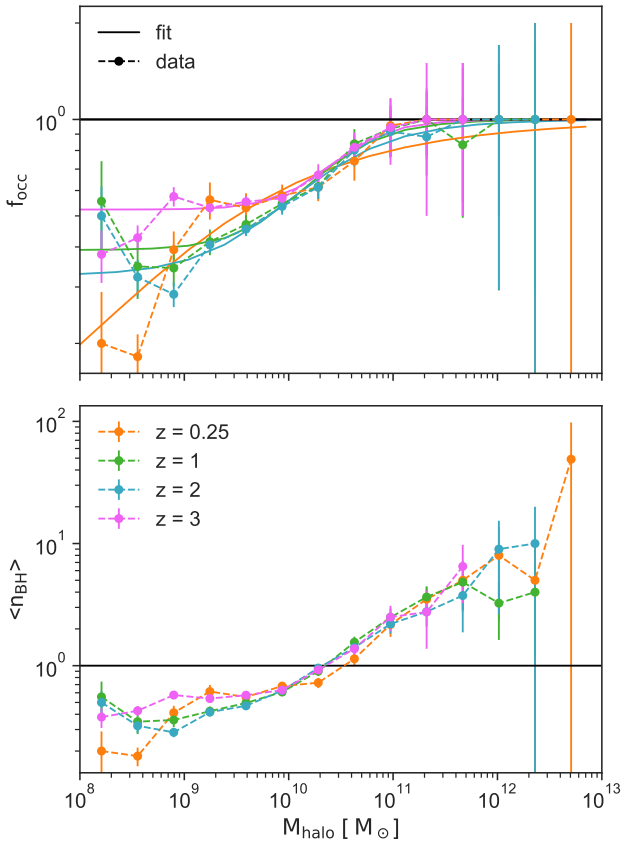

Figure A1. Fraction of halos that contain at least one BH [top] and average number of BHs per halo[bottom] as a function of halo mass M_{halo}. Solid lines on the top panel denote a fit of Eq. 3, with free parameters at each redshift listed in Table A1. Dashed lines connect data points. Error bars show Poisson errors.